Available online at www.sciencedirect.com
SCIENCE DIRECT®
Journal of Power Sources 141 (2005) 369–385
JOURNAL OF POWER SOURCES
www.elsevier.com/locate/jpowsour

Activated-carbon electric-double-layer capacitors: electrochemical characterization and adaptive algorithm implementation

Mark W. Verbrugge[a,*], Ping Liu[b], Souren Soukiazian[b]

[a] *Materials and Processes Lab, General Motors Corporation, R&D Center, 30500 Mound Road, P.O. Box 9055, Warren, MI 48090-9055, USA*
[b] *HRL Laboratories, LLC, 3011 Malibu Canyon Road, Malibu, CA 90265, USA*

Received 5 September 2004; accepted 27 September 2004
Available online 9 December 2004

Abstract

An activated-carbon electric-double-layer capacitor is characterized and an adaptive algorithm is derived and implemented that is commensurate with potential traction applications of these energy storage devices. The electrochemical characterization relies on a simplified equivalent circuit interpretation extracted from a more-complete mathematical representation of the capacitor system. In addition to the high power capability and potentially low costs of this class of capacitors, we clarify the substantial invariance of the device performance with respect to temperature, a distinct advantage over battery systems. The robustness of the equivalent circuit in terms of capturing the salient features of the experimental data over the temperature and voltage range of interest enables the formulation of a model-reference adaptive algorithm. The algorithm developed and implemented in this work is fully recursive in that the only variables required for on-line regression are those of the previous time step and the current time step. Successful comparisons of the algorithm's adapted state of charge and power predictions provide an initial validation of the algorithm.

Keywords: Capacitor; State of charge; Activated carbon; Adaptive algorithm; Control; Power capability

1. Introduction

Although activated-carbon electric-double-layer capacitors yield high power over a broad temperature range and consist of potentially low-cost materials, they have not been characterized sufficiently from the viewpoint of automotive traction applications, and the control of these systems has not been studied in the context of formal control algorithms (i.e., optimal estimators and adaptive filters). The motivation behind determining a battery's (i) state of charge (SOC), (ii) state of health (SOH), and (iii) power capability (PC) for both discharge and charge has been described recently [1]. The same motivation applies to electric-double-layer-based capacitors. The SOC corresponds to the stored charge available to do work relative to that available after the electrochemical system has been fully charged and can be viewed as a thermodynamic quantity. SOH refers to how well the system is functioning relative to its nominal (rated) and end (failed) states. The same three characteristics (SOC, SOH, and PC) are required for the rational integration of electrochemical-based energy storage devices. A general survey of electrochemical capacitors can be found in Conway's text [2]. In this work we are specifically interested in capacitors based on high surface area, activated-carbon electrodes. Helpful reviews concerning the utility and characterization of these systems can be found in [3–5]. In the 2002 paper by Chu and Braatz [4], the SAFT carbon-based capacitor was shown to be the best performing of the non-aqueous-solvent systems investigated by the authors, as shown clearly in the Ragone plot (specific energy plotted against specific power) in Fig. 3 of their paper. The SAFT capacitor is further characterized in this communication. Our goal is to understand sufficiently the underlying physical chemistry of these devices so as to allow for vehicle integration and control. Related to automotive propul-

* Corresponding author. Tel.: +1 586 986 2010; fax: +1 586 986 3091.

0378-7753/$ – see front matter © 2004 Elsevier B.V. All rights reserved.
doi:10.1016/j.jpowsour.2004.09.034

sion systems, most texts covering control theory will treat motor control and feedback systems associated with vehicle speed control, little attention has been given to the adaptive control of battery systems [1,6,7]) or electric-double-layer capacitors [8].

We have chosen to investigate this class of capacitors because they show potential for providing a much higher specific power (kW kg^{-1}) and power density (kW l^{-1}) than advanced batteries at a much lower cost ($ per kW). The material costs should be much lower than that of advanced batteries, as the primary costs corresponds to activated carbon for the electrodes, aluminum for the current collectors, and a salt in propylene carbonate or acetonitrile (or an equivalent non-aqueous solvent) for the electrolyte phase [9,10,14]. A large effort is now underway in the electrochemical-materials research community to reduce the cost of the activated carbon [11–13], the remaining high-cost material in these systems. Methods by which one can assess the microstructure and pore-size distribution of the activated carbons relevant to capacitor applications are reviewed and discussed in [15]. In addition, because of the high specific power and power density of these capacitor systems, it may be possible to eliminate the dc/dc converter used in propulsion systems for controlling voltages between energy storage subsystems; a dc/dc converter is used, for example, when a battery is placed in parallel with a fuel cell [14].

This paper is organized as follows. Following a brief overview of the experimental tools employed, the theoretical underpinnings and governing equations utilized in the characterization tests and adaptive algorithm are presented. For detailed mathematical modeling of electric-double-layer capacitor systems and references to both classical and recent work in this area [16–25] are quite helpful. In the last portion of this paper, the results are discussed for the characterization studies, the use of the current–voltage relations as an adaptive filter is examined, and finally the adaptive algorithm is implemented to post-process data.

2. Experimental

The capacitor was acquired from Saft America. It has a nominal capacitance of 3500 F and a maximum voltage of 2.8 V. Electrochemical tests were performed on an Arbin BT2000 battery testing system (Arbin Instruments, College Station, TX). Generally, data acquisition rates of approximately 1 point per 100 ms were used. Tests were conducted at −30, 0, 25, and 45 °C. Temperature control was provided by a Tenney environment chamber (Model Tenney20, Lunaire, Williamsport, PA). At each temperature, an energy test, a charge power test and a discharge power test were performed as summarized in Table 1. Prior to a test, the capacitor was allowed to equilibrate at a given temperature for 4 h.

Table 1
Characterization test procedures

Energy (SOC) test	
1	Equilibrate at 0 V
2	Charge at 100 A to 1.7 V
3	Step to 0 A for 3 min; record V_0
4	Discharge at 1 A until 0 V is obtained
5	Repeat step 2 in increments of 0.1–2.4 V (1.7, 1.8, 1.9, . . ., 2.4 V)
Discharge power test	
1	Equilibrate at 0 V
2	Charge at 100 A to 1.7 V
3	Step voltage to 1.4 V for 5 s
4	Step to 0 A for 3 min; record V_0
5	Repeat step 2 in increments of 0.1–2.8 V (1.7, 1.8, 1.9, . . ., 2.4 V)
Charge power test	
1	Equilibrate at 0 V
2	Charge at 100 A to 1.7 V
3	Step voltage to 2.8 V for 5 s
4	Step to 0 A for 3 min; record V_0
5	Repeat step 2 in increments of 0.1–2.8 V (1.7, 1.8, 1.9, . . ., 2.4 V)

These capacitors normally operate between the maximum voltage and one-half that value. The maximum voltage for this system is 2.8 V, and the lowermost voltage applied was 1.4 V.

2.1. Energy test

The capacitor was discharged to 0 V and held at that voltage for 300 s. It was subsequently charged to a preset potential of 1.7 V at a constant current of 100 A followed by an open-circuit rest for 180 s. The capacitor was then discharged to 0 V at a constant current of 1 A. This sequence was repeated for a series of preset potentials at 0.1 V increment from 1.8 to 2.4 V.

2.2. Discharge power test

The capacitor was discharged to 0 V and held at that voltage for 300 s. It was then charged to a preset potential of 1.7 V at a constant current of 100 A. Subsequently, a constant voltage of 1.4 V was applied for 5 s and the capacitor was allowed to rest at open-circuit voltage for 180 s. This sequence of test was repeated for a series of preset potentials at 0.1 V increment from 1.8 to 2.4 V.

2.3. Charge power test

This test was similar to the discharge power test, except a constant voltage of 2.8 V was applied instead of 1.4 V.

3. Equivalent circuit analysis and adaptive algorithm

The model used for the characterization analysis and the adaptive algorithm consists of two parts. There is an electrical circuit model that is employed to describe the relationship between the currents and voltages observed at the terminals of the capacitor (giving rise to the voltage-based SOC_V) and a coulomb-accumulation model that describes the open-circuit voltage-based on the history of currents seen by the capacitor

(giving rise to the coulomb-counting-based SOC_C), which can include self discharge and current inefficiency on charge. The electrical circuit model is illustrated Fig. 1. This equivalent circuit is used to extract a current–voltage expression, which is then employed to characterize the capacitor. In addition, the current–voltage expression forms the basis for the voltage-based SOC_V. It should be recognized that even the more complex equivalent circuit shown in the upper schematic of Fig. 1 constitutes a greatly simplified approach to modeling a capacitor system [25], but the model will prove useful for the purposes of an adaptive transversal filter.

3.1. Recursive voltage expression

By summing the voltage around the circuit shown in Fig. 1, one obtains:

$$V = \frac{Q}{C} + IR, \tag{1}$$

where the relationship between the charge on the capacitor and the associated current is:

$$I = \frac{\mathrm{d}Q}{\mathrm{d}t}.$$

The initial condition for V or I corresponds to:

$$V(0) = \frac{Q(0)}{C} + I(0)R.$$

We shall assume that the values of R and C do not change substantially over the time scale RC. Differentiation of Eq. (1) leads to:

$$\frac{\mathrm{d}V}{\mathrm{d}t} = \frac{I}{C} + R\frac{\mathrm{d}I}{\mathrm{d}t}.$$

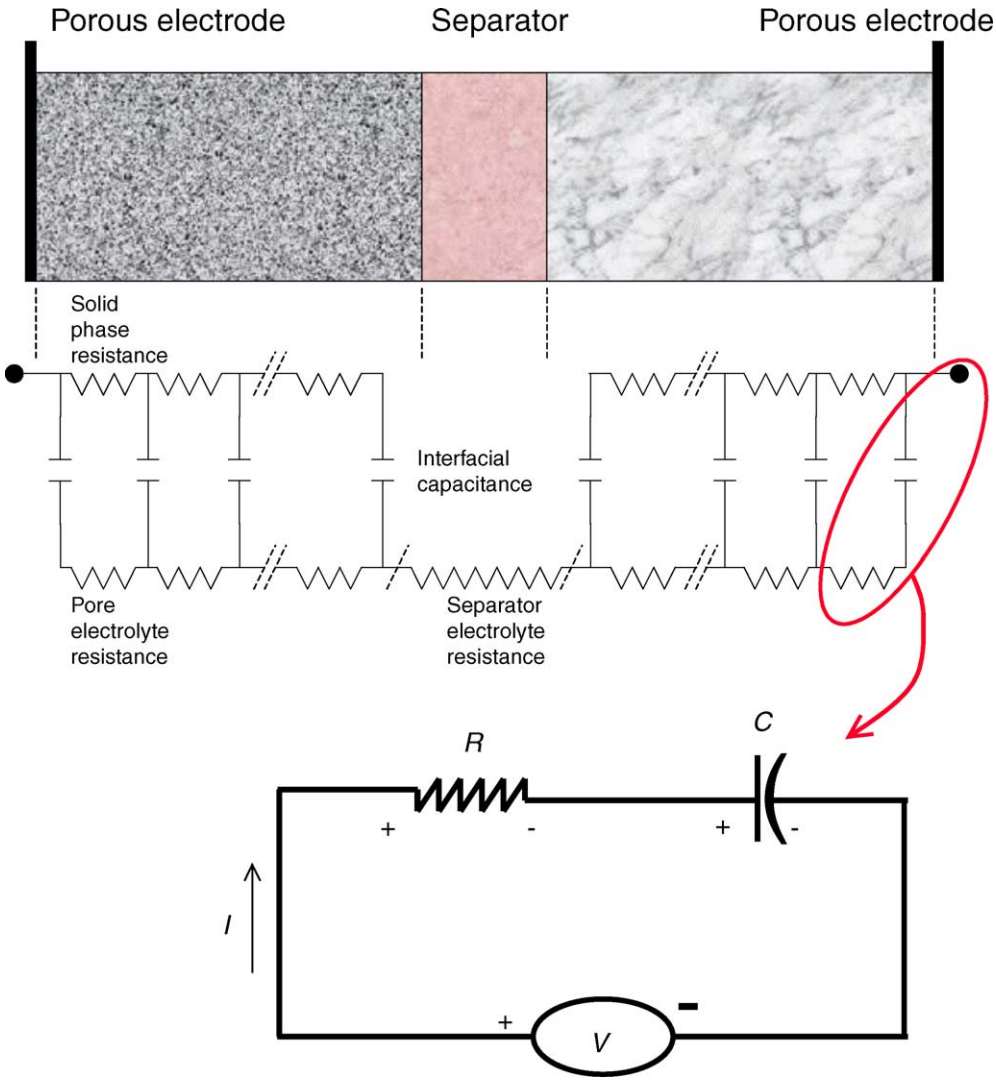

Fig. 1. Equivalent circuit representation. The upper figure provides an equivalent circuit for a capacitor dominated by ohmic drop and comprising ideal capacitive behavior at the electrode–electrolyte interface. The simplified equivalent circuit used to construct the adaptive filter is then extracted from the upper figure as indicated.

The solution to this equation for a variable current source is:

$$V = \frac{Q(0)}{C} + IR + \frac{1}{C}\int_{\zeta=0}^{\zeta=t} I|_{\zeta}\mathrm{d}\zeta. \tag{2}$$

For constant current discharge,

$$V = \frac{Q(0)}{C} + IR + \frac{It}{C}. \tag{3}$$

This equation is used to extract the capacitance versus open-circuit voltage relationship (Figs. 3 and 4). Note that the open-circuit voltage V_0 corresponds to Q/C in the absence of current flow.

The first step in constructing the voltage-based portion of the SOC algorithm is to convert the integral (2) into a recursive relation. We shall work through the first few time steps to elucidate the general pattern and then provide the necessary relation. Initially, $t = t_0 = 0$, and Eq. (2) can be descretized as:

$$V|_0 = Q|_0\frac{1}{C} + I|_0 R.$$

After the first time step, $t = t_1$, and

$$V|_1 = (t_1 - t_0)\frac{I|_1 + I|_0}{2}\frac{1}{C} + I|_1 R + (V|_0 - I|_0 R),$$

where the integrand I has been approximated by the average of its beginning and ending values of the time step. After the second time step, $t = t_2$, and

$$V|_2 = (t_2 - t_1)\frac{I|_2 + I|_1}{2}\frac{1}{C} + I|_2 R + (V|_1 - I|_1 R),$$

and this general pattern holds for time step N:

$$V|_N = (t_N - t_{N-1})\frac{I|_N + I|_{N-1}}{2}\frac{1}{C} + I|_N R + (V|_{N-1} - I|_{N-1}R). \tag{4}$$

Thus, to determine the voltage at time N, $V|_N$, one only needs the present value of the current and the previous time-step values for the current and voltage. Consequently, Eq. (4) is a recursive transformation of Eq. (2) into a descretized time domain. The next section will formulate an adaptive procedure for the estimation of R and C from a history of currents and voltages, which allows for the state estimation of the capacitor.

3.2. Weighted recursive least square for the estimation of R and C

Eq. (4) is a linear relation as formulated, and least squares methods can be used to minimize the error between the predicted voltage V and the measured voltage V_{meas} by appropriate adjustment of R and C as part of a parameter estimation scheme. Reviews on the substantially interdependent fields of recursive identification, adaptive filters, optimal estimators, and model-reference adaptive systems (MRAS's) can be found in [26–32]. The following definitions will streamline notation:

$$x_1 = I_t - I_{t-\Delta t} \qquad x_2 = (I_t + I_{t-\Delta t})\tfrac{\Delta t}{2}$$
$$m_1 = R \qquad m_2 = \tfrac{1}{C}$$
$$y = V_{\mathrm{meas},t} - V_{\mathrm{meas},t-\Delta t}$$

Eq. (4) can now be recast as:

$$y = m_1 x_1 + m_2 x_2,$$

and the error ε that we seek to minimize corresponds to:

$$\varepsilon = \sum_{j=1}^{N} w_j[y_j - (m_1 x_{1,j} + m_2 x_{2,j})]^2.$$

Time t corresponds to index $j = N$ in the above. Two equations for the two parameters to be extracted can be generated by setting the partials $\partial\varepsilon/\partial m_1$ and $\partial\varepsilon/\partial m_2$ to zero. This leads to:

$$m_1 = \frac{1}{\mathrm{Det}}(V_{1,y}V_{2,2} - V_{2,y}V_{1,2}) \quad \text{and}$$
$$m_2 = \frac{1}{\mathrm{Det}}(V_{2,y}V_{1,1} - V_{1,y}V_{2,1}), \tag{5}$$

where the matrix determinant Det is given by:

$$\mathrm{Det} = V_{1,1}V_{2,2} - V_{1,2}^2.$$

The variances corresponds to:

$$V_{u,v}|_N = \left(s_{u,v}|_N - \frac{s_u|_N s_v|_N}{s_w|_N}\right)\frac{1}{s_w|_N}, \tag{6}$$

in which the sums refer to:

$$s_w = \sum_{j=1}^{N} w_j, \qquad s_u = \sum_{j=1}^{N} w_j u_j,$$
$$s_v = \sum_{j=1}^{N} w_j v_j, \qquad s_{u,v} = \sum_{j=1}^{N} w_j u_j v_j,$$

and u and v refer to x_1, x_2, or y. It should be noted that the matrix system is symmetric, $V_{1,2} = V_{2,1}$. Variances have been used in these expressions, along with the normalization associated with the division by s_w in order to keep the resulting matrix elements nearer to unity (i.e., well scaled).

Before making the summations recursive, we address the weight factor w_j. There are two reasons why one would want to weight data sets differently. First, some observations may be subject to greater disturbance; here, a disturbance refers to a phenomenon not accounted for in the system model. For example, the onset of secondary reactions during capacitor charging [16] may lead one to discount the charge observations relative to those of discharge, as the impact of the secondary reactions is not treated in the model equations. Second, newer observations are generally more important than older observations in determining the state of the system,

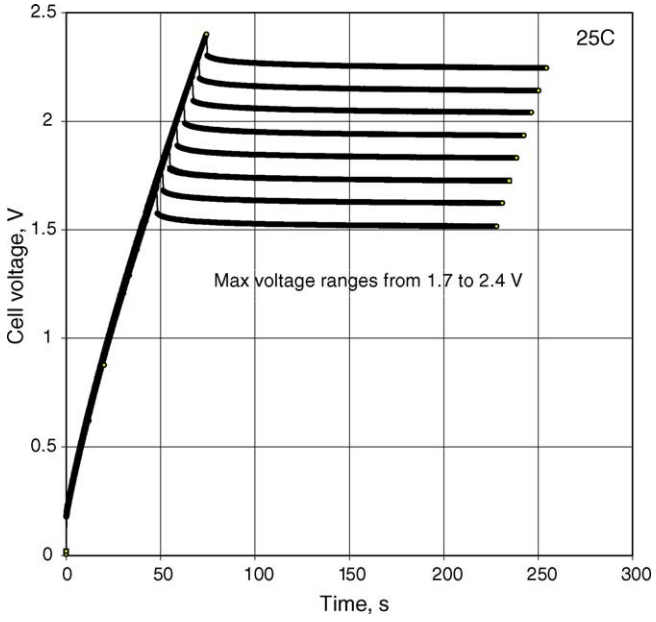

Fig. 2. Energy test results for 25 °C data. The cell is charged at 100 A to the indicated maximum voltage, after which the current is set to 0 A for 3 min, and then a 1 A discharge is used to determine the coulombs stored in the capacitor at the equilibrium voltage V_0 (discharge part not shown), allowing for the determination of the cell capacitance as a function of V_0 (cf. Table 1.) Analogous plots were obtained at −30, 0, and 45 °C.

and therefore, should usually be given a larger weight factor relative to older observations. For these two reasons, we decompose the weight factor into a time-weighting factor λ and a general weight factor γ; the latter of which can be used

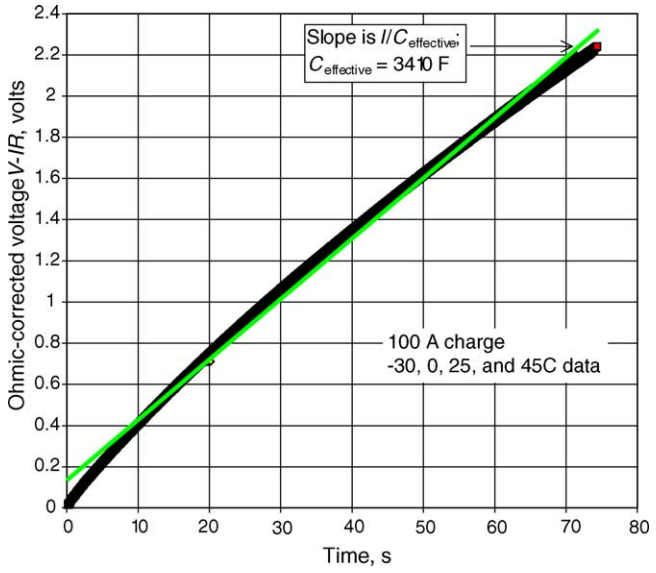

Fig. 3. Ohmic-corrected voltage versus time for 100 A charge (cf. Fig. 2). The variation with temperature is comparable to the experimental resolution. The capacitance fit to the straight line corresponds to 3410 F (cf. Eq. (3)), which is consistent with the 1 A discharge data shown in Fig. 4, both in terms of the value for the fit capacitance and the observed invariance of the capacitance with temperature. The resistances employed to form *V–IR* are plotted in Fig. 8.

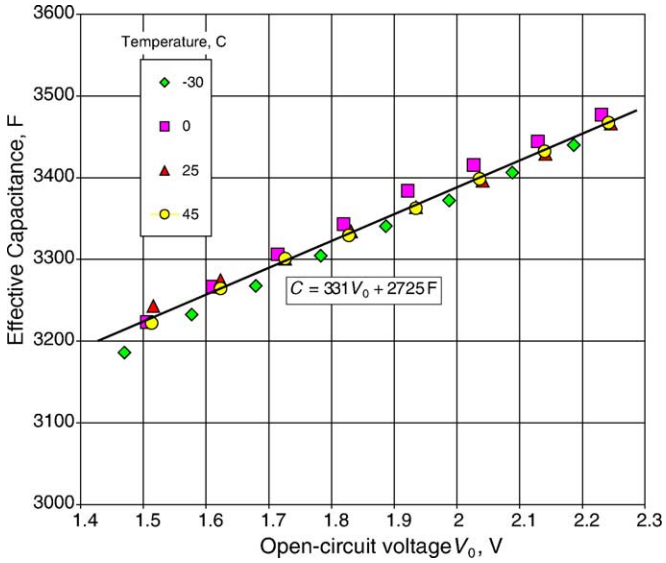

Fig. 4. Cell capacitance determined by energy test (1 A discharge) as a function of the open-circuit voltage and temperature.

to associate a specified weighting of selected events (e.g., discharge events over charge events). Hence,

$$w_j = \gamma_j \lambda^{N-j}. \tag{7}$$

It can be shown that the use of λ^{N-j} yields an exponential decay in the influence of past data points on the determination of the current value of m_1 and m_2:

$$\lambda^{N-j} = e^{\ln \lambda^{N-j}} = e^{(N-j)\ln\lambda} \approx e^{-(N-j)(1-\lambda)}, \qquad \text{for } \lambda \to 1.$$

Hence, a data point taken 100 s prior to the current point has less than 40% of the impact on the regression analysis relative to that of the current point. A data point taken 500 s prior to the current point has less than 1% of the impact on the regression relative to that of the current point. More-complete discussions on exponential forgetting can be found in Section 5.6.1 of Ljnug and Söderström [29], Section 6.2 of Anderson and Moore [31], and Sections 5.3 and 5.4 of Kulhavý [32]. The summations are now made recursive with the following definitions:

$$\begin{aligned} &s_w|_N = \gamma_N + \lambda(s_w|_{N-1}), \\ &s_u|_N = \gamma_N u_N + \lambda(s_u|_{N-1}), \quad s_v|_N = \gamma_N v_N + \lambda(s_v|_{N-1}), \\ &\text{and} \\ &s_{u,v}|_N = \gamma_N u_N v_N + \lambda(s_{u,v}|_{N-1}), \end{aligned} \tag{8}$$

with $s_{u,v} = s_{v,u}$. Initially,

$$\begin{aligned} &s_w|_1 = \gamma_1, \\ &s_u|_1 = \gamma_1 u_1, \quad s_v|_1 = \gamma_1 v_1, \quad \text{and}. \\ &s_{u,v}|_1 = \gamma_1 u_1 v_1 \end{aligned} \tag{9}$$

At this point, the equations needed to regress the parameters m_1 and m_2 have been fully stated. At the beginning of

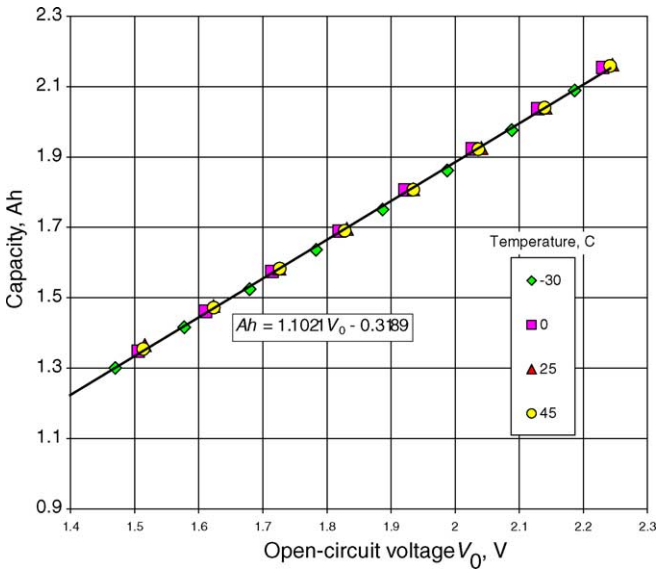

Fig. 5. Cell capacity (Ah) determined by energy test (1 A discharge) as a function of the open-circuit voltage and temperature.

each time step, the recursive sums (8) are calculated (Eq. (9) for the first time step), which are then substituted in the variances (6); upon determining all variances, the parameters m_1 and m_2 are deduced by means of Eq. (5), thereby providing C and R.

3.3. State-of-charge (SOC)

The previous section provided for the extraction of C and R from a data stream provided the determinant reflects a well-posed equation system. We now use this information along with coulomb counting to construct the SOC algorithm. When all of the current goes to charging or discharging the electric-double-layer associated with the surface of the porous electrodes of the capacitor, Eq. (2) can be rearranged such that:

$$Q = Q(0) + \int_{\zeta=0}^{\zeta=t} I|_\zeta \mathrm{d}\zeta = C(V - IR),$$

where Q is the magnitude of the charge on the (symmetric) capacitor electrodes. We define the voltage-based SOC, SOC_V, in terms of the minimum charge on the capacitor $Q_{\min}$ relative to its maximum value $Q_{\max}$ allowed under normal operating conditions,

$$\mathrm{SOC}_V = \frac{Q - Q_{\min}}{Q_{\max} - Q_{\min}} = \frac{C(V - IR) - Q_{\min}}{CV_{\max}|_{I=0} - Q_{\min}} = \frac{V - IR - V_{\min}|_{I=0}}{V_{\max}|_{I=0} - V_{\min}|_{I=0}},$$

where $Q_{\min}$ and $Q_{\max}$ correspond to the minimum and maximum voltages ($V_{\min}$ and $V_{\max}$, respectively) under zero current conditions. In vehicle applications, the power electronics (i.e., the power inverter) used to convert the dc current associated with the energy storage device (e.g., a battery, fuel cell, or capacitor) to ac current for the electric machines require that $V_{\min} \geq 0.5\, V_{\max}$ in order that the power inverter maintain an acceptable efficiency. Thus, for the figures presented herein, $V_{\min}$ is set to zero in formulating the SOC, and we investigate SOC's ranging from 50 to 100 percent in the power capability analyses ($1.4 \leq V_0 \leq 2.8$ V); 100 percent SOC and $V_{\max}$ are taken to correspond to 2.8 V, which implies that $V_0 = 1.4$ V refers to 50% SOC.

We can also calculate an SOC based on coulomb counting so as to construct a current-based SOC, SOC_I,

$$\mathrm{SOC}_I(t) = \mathrm{SOC}(t - \Delta t) + \left(\frac{I_t + I_{t-\Delta t}}{Q_{\max} - Q_{\min}}\right)\frac{\Delta t}{2} = \mathrm{SOC}(t - \Delta t) + \frac{1}{C}\left(\frac{I_t + I_{t-\Delta t}}{V_{\max}|_{I=0} - V_{\min}|_{I=0}}\right)\frac{\Delta t}{2}. \quad (10)$$

Both the voltage and current-based SOC's contain useful information, and a weighted average is thus rendered as the final (combined) SOC,

$$\mathrm{SOC} = w\mathrm{SOC}_I + (1 - w)\mathrm{SOC}_V, \quad (11)$$

with the weight factor w chosen to be closer to 1 for enhanced stability and closer to zero for increased responsiveness. Unless otherwise noted, a value of $w = 0.999$ was used in this work. It should be noted that w must be viewed in the context of the time per point, as the coulomb counting includes time integration, unlike the more-responsive voltage-based SOC. Upon inspection of the formulas for SOC_V and SOC_I, we note that SOC_V utilizes the adapted resistance R and SOC_I relies on the adapted value for C, and in this context both SOC_V and SOC_I are adaptive quantities as is the composite value of SOC. In addition, it is important to note that in the formulation of Eq. (10) for SOC_I, we increment from the previous value of SOC (not SOC_I), thereby linking explicitly the current-based SOC to the voltage-based SOC. In summary, the adaptive algorithm comprises specifically Eqs. (4)–(11).

3.4. Power capability

The maximum discharge power can be expressed as:

$$P_{\max,\,\mathrm{discharge}} = IV = IV_{\min}.$$

That is, when the capacitor voltage obtains its lowest acceptable value, the max discharge power results. First, we consider the available instantaneous power; i.e., the power available before the charge on the capacitor is depleted significantly by the discharge event. In this case, $V = V(0) + IR$, where $V(0)$ is the system voltage at zero current immediately prior to the discharge [$V(0) = Q(0)/C$, cf. Eq. (2)], and

$$P_{\max,\,\mathrm{discharge}} = IV_{\min} = \frac{[V_{\min} - V(0)]}{R}V_{\min}. \quad (12)$$

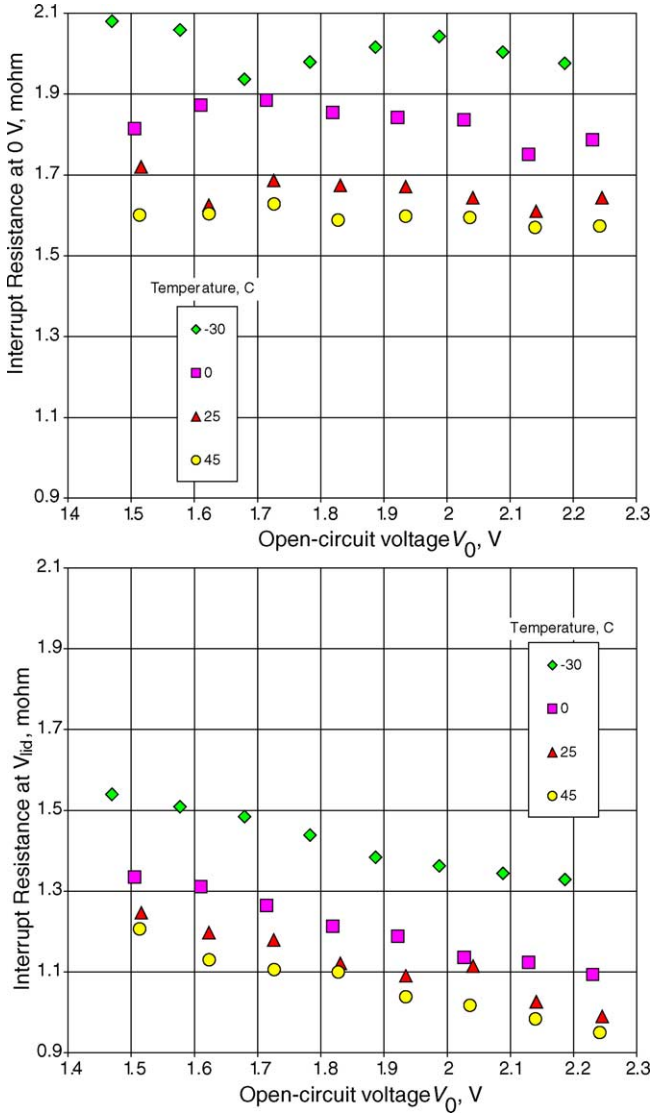

Fig. 6. Interrupt resistance at 0 V (upper plot) and at the voltage lid (lower plot) as a function of the open-circuit voltage and temperature.

Similarly, the instantaneous charge power for the ohmic battery is given by:

$$P_{\text{max, charge}} = IV_{\max} = \frac{[V_{\max} - V(0)]}{R} V_{\max}. \tag{13}$$

The ohmic battery does not address transient effects, which are important for times that are greater than ~0.01 *RC*. In this case, Eq. (4) can be inverted to solve for the current, and consequently, we can calculate the maximum charge and discharge powers available for the time interval Δt:

$$I|_t = \frac{V_t - [I_{t-\Delta t}\Delta t/(2C)] - (V - IR)_{t-\Delta t}}{R + [\Delta t/(2C)]},$$

$$P_{\text{max, discharge}}(\Delta t) = IV_{\min}$$

$$= \left[\frac{V_{\min} - [I_{t-\Delta t}\Delta t/(2C)] - (V - IR)_{t-\Delta t}}{R + [\Delta t/(2C)]}\right] V_{\min},$$

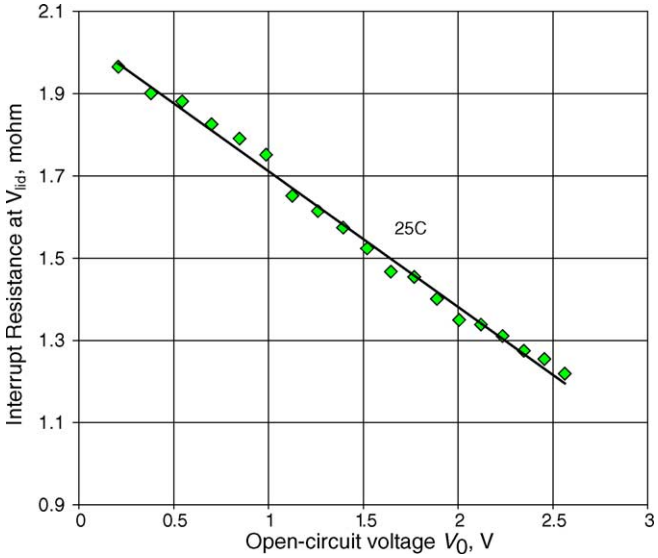

Fig. 7. Expanded analysis of the interrupt resistance at the voltage lid. The approximately linear trend in the interrupt resistance versus open-circuit voltage depicted in Fig. 6 is seen to apply over a broad voltage range.

and $P_{\text{max, charge}}(\Delta t) = IV_{\max}$

$$= \left[\frac{V_{\max} - [I_{t-\Delta t}\Delta t/(2C)] - (V - IR)_{t-\Delta t}}{R + [\Delta t/(2C)]}\right] V_{\max}. \tag{14}$$

As $\Delta t \to 0$, the transient power calculations match those of the instantaneous power calculation. To implement the

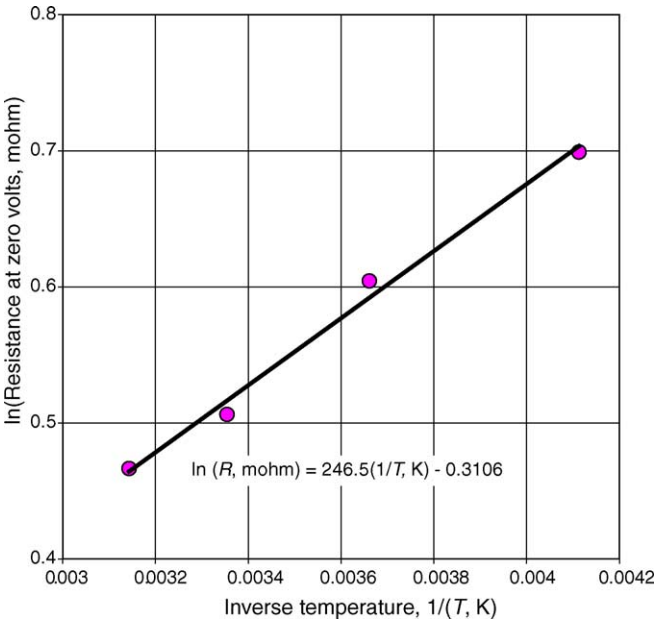

Fig. 8. Resistance variation with absolute temperature. The slope yields an activation energy of 2.0 kJ mol^{-1}. The resistance values correspond to an average of the resistance (at the indicated temperature) shown in the upper plot of Fig. 6. From left to right, the temperatures correspond to 45, 25, 0, and −30 °C.

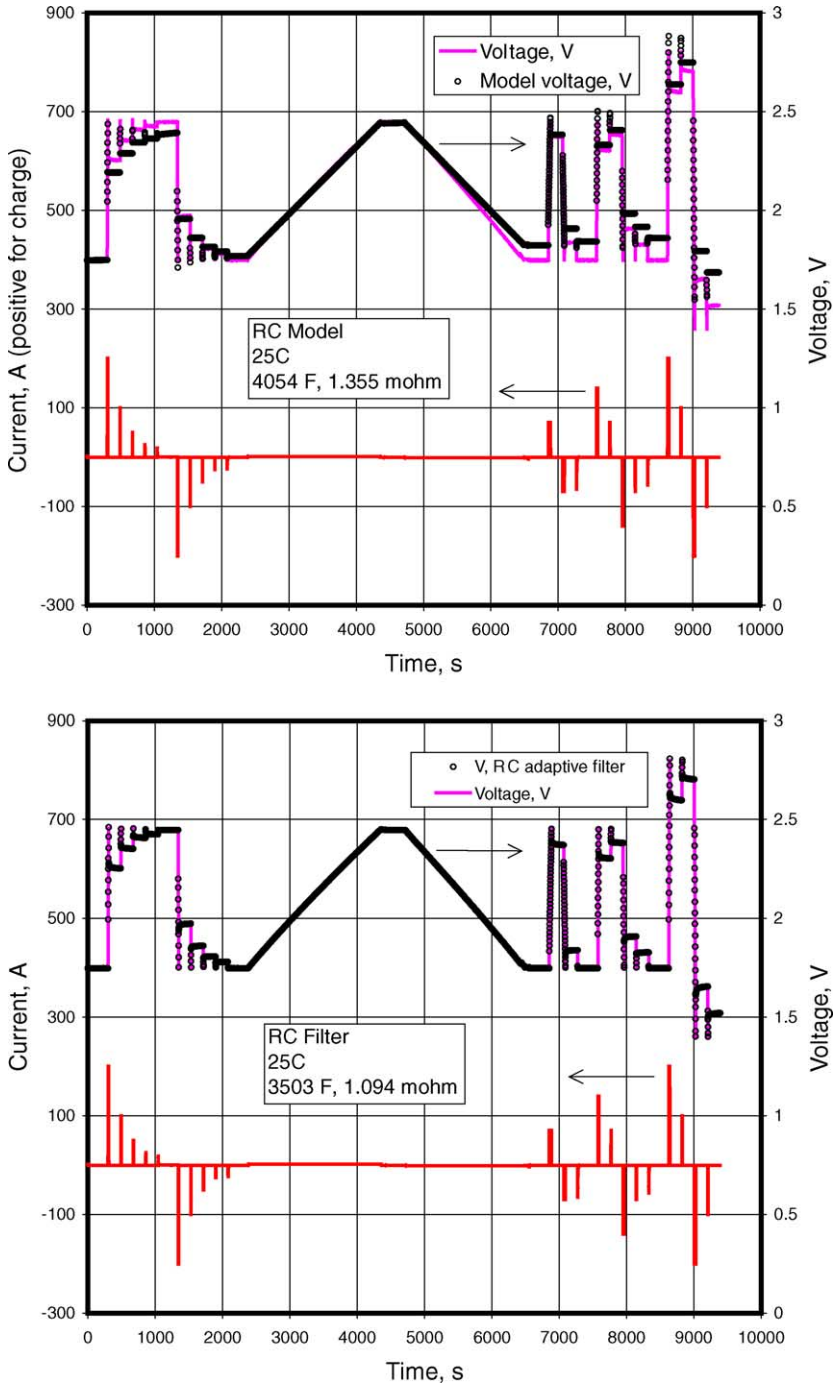

Fig. 9. Comparison of model results and adaptive filter. Upper plot: model results. Lower plot: adaptive filter. Calculations for both plots employed Eq. (4). For the upper plot, $V|_{N-1}$ in Eq. (4) corresponds to the previously calculated voltage, whereas $V|_{N-1}$ corresponds to the previously measured voltage for the lower plot. The parameters R and C were fit by least squares analysis, with each point receiving equal weighting.

transient equations, the respective powers are calculated immediately after the algorithm has been employed to finish the SOC determination at time t. In this case, quantities calculated or measured at time t are then stored in the variables listed in the respective power expressions at time $t - \Delta t$. Then one must state the duration corresponding to the desired estimate for power. For example, if we want to know the power estimates 2 s from "now", then the current measured and extracted values are placed in the $t - \Delta t$ quantities, t and Δt are set to 2 s, and the right sides of the above equations yield the desired power estimates. Bounds on the current magnitudes should also be observed in actual applications; that is, the power capability may be limited by a maximum current specified for the capacitor so as to avoid degradation.

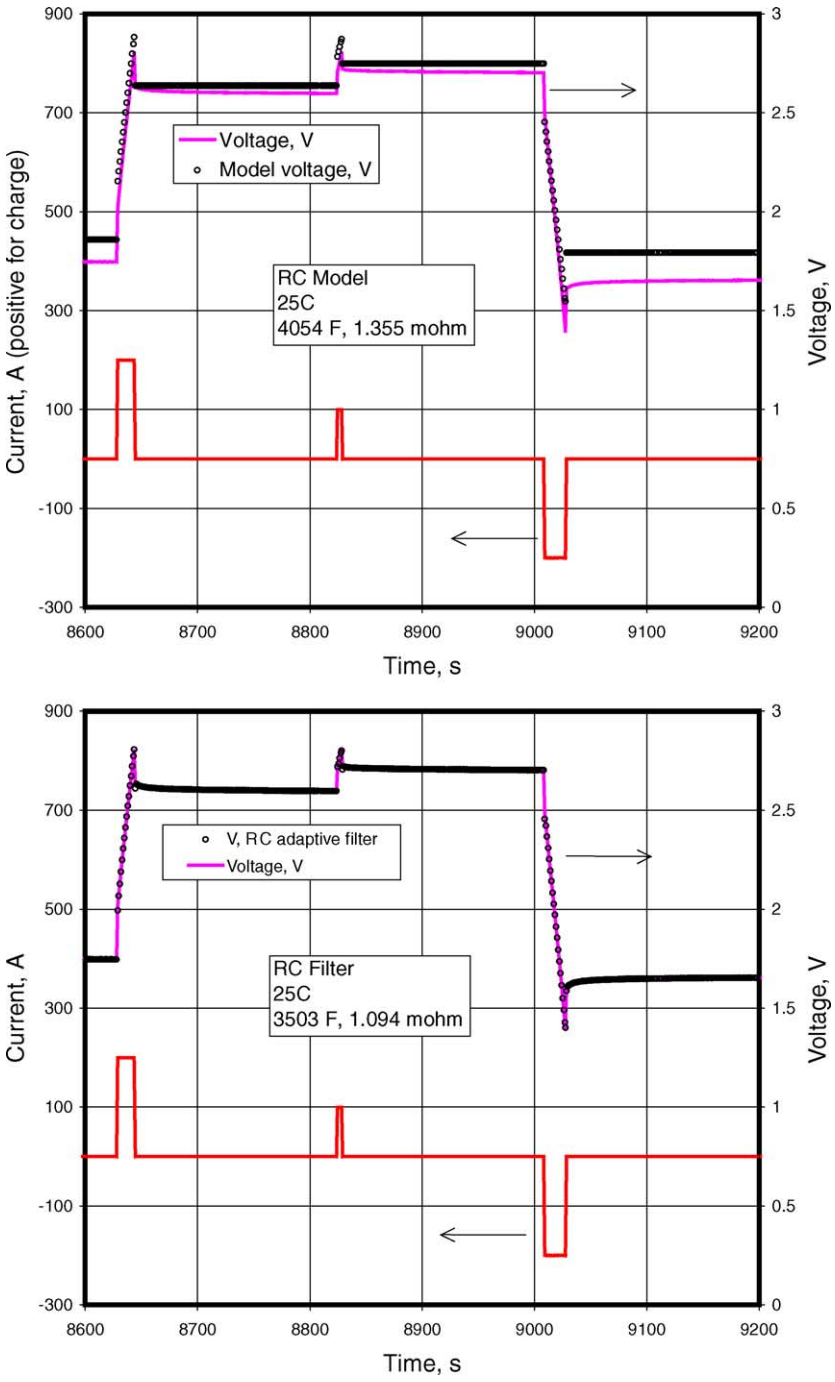

Fig. 10. Expanded view of plots shown in Fig. 9. The nearly linear variation in the cell voltage during the constant current charge and discharge at 200 A magnitude is clearly evident.

4. Results and discussion

4.1. Characterization tests

The first step in constructing an adaptive algorithm is to characterize the system. This allows one to determine the suitability of selected physical models (e.g., the simplified equivalent circuit depicted in Fig. 1) and to place reasonable bounds on the parameter values. This latter attribute is significant, for it enables one to determine when the regressed parameters take on reasonable values, indicating robust performance of the algorithm and the device. The three types of characterization tests implemented in the work are described in Table 1.

The energy test can be used to measure the cell capacitance and coulombic capacity, rendered in units of Ah so as

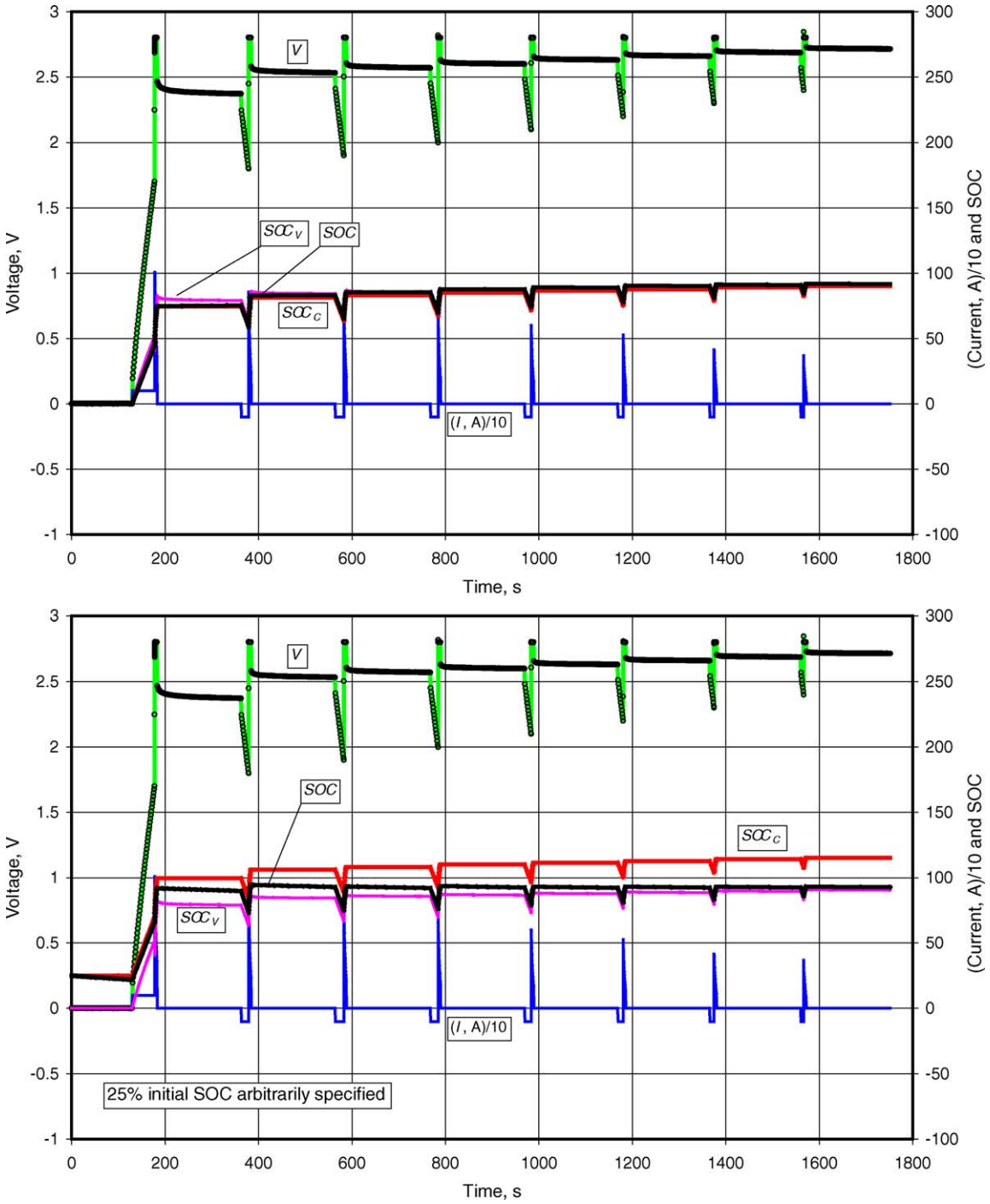

Fig. 11. Charge power test (cf. Table 1). The extracted state of charge (SOC) from the adaptive algorithm is indicated, as is the voltage-based contribution (SOC_V) and that corresponding to purely coulomb counting (SOC_C). The effect of the specified initial SOC and the algorithm convergence behavior is clarified by comparing the upper and lower plots; an erroneous 25% initial SOC was specified in the lower plot.

to be consistent with battery nomenclature. Data for the constant current (100 A) charge to the various voltage lids, followed by the 180 s open-circuit stand, are provided in Fig. 2 for the 25 °C condition. As indicated in Fig. 3, the effect of temperature on the data as plotted was difficult to discern. After open-circuit stand, the open-circuit potential V_0 is recorded. It then remains to determine how much charge resides on the electrodes, and for this reason a low current discharge of 1 A is performed to 0 V. The capacitance C is calculated from $C = Q/V_0$, where Q is the charge passed during the 1 A discharge. The measured capacitance C and capacity in Ah are plotted in Figs. 4 and 5, respectively, over a temperature range of interest for automotive applications. The equilibrium capacitance plotted in Fig. 4 is similar to the

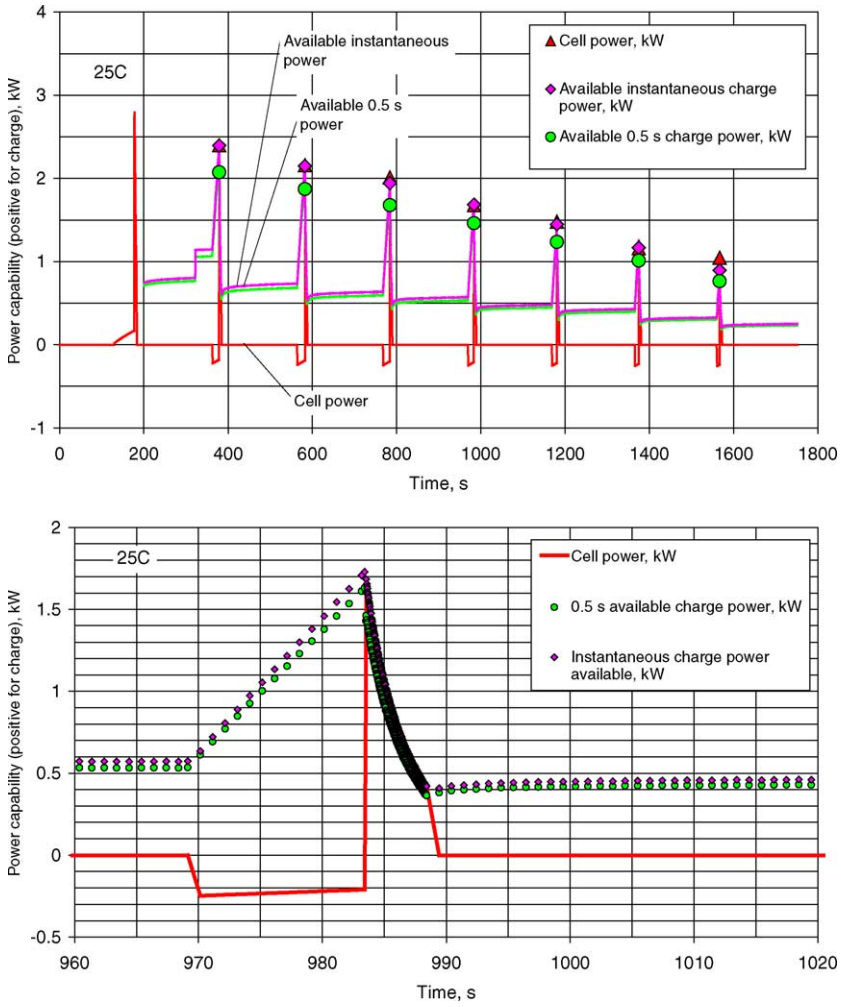

Fig. 12. Available charge power analysis. The algorithm utilizes the current and voltage traces shown in the upper plot of Fig. 11 to produce the available power results depicted above. The cell power is the current multiplied onto the voltage. The lower plot expands the abscissa of the upper plot around 990 s. The key conclusion is that the available power predictions rendered by the recursive algorithm follow closely the measured power through the current reversal at 984 s. For this analysis, $\lambda = 0.995$.

effective capacitance extracted from the slope of the 100 A charge data plotted in Fig. 3; Eq. (3), with $Q = 0$ (corresponding to a zero initial voltage for the constant current charge), was used to approximate the capacitance. For both methods of extracting a cell capacitance, little temperature variation is observed. The curvature in the voltage versus time curve in Fig. 3 is consistent with porous electrode analyses [16].

When the current is changed from 0 to 100 A at the start of the experiment corresponding to Fig. 2, and when the current is switched from 100 A to zero upon reaching the voltage lid, an interrupt resistance can be ascertained. Impedance due to ionic diffusion complicates the analysis; for our purposes, we simply plot $\Delta V/\Delta I$ as an interrupt resistance in Fig. 6. At 0 V, the interrupt resistance is seen to be nearly invariant with SOC (i.e., V_0), and the interrupt resistance decreases in a nearly monotonic manner with SOC, a feature more fully examined in Fig. 7. A succinct explanation for the monotonic trend in the interrupt resistance seen in the lower panel of Fig. 6, and in Fig. 7, remains an open question. When the logarithms of interrupt resistances near 0 V (values averaged over the SOC for each temperature) are plotted against the inverse of the absolute temperature (Fig. 8), we extract a rather low activation energy of 2 kJ mol^{-1}. This low activation energy and the relative invariance in the capacitance with temperature help to explain why activated-carbon electric-double-layer capacitors are of interest for automotive applications, as these capacitors maintain their power capability at lower temperatures much more so than batteries.

4.2. Transversal filter

The prior characterization of the capacitor indicates that the RC equivalent circuit depicted in Fig. 1 captures many of the features of the potential–current relationship. While the

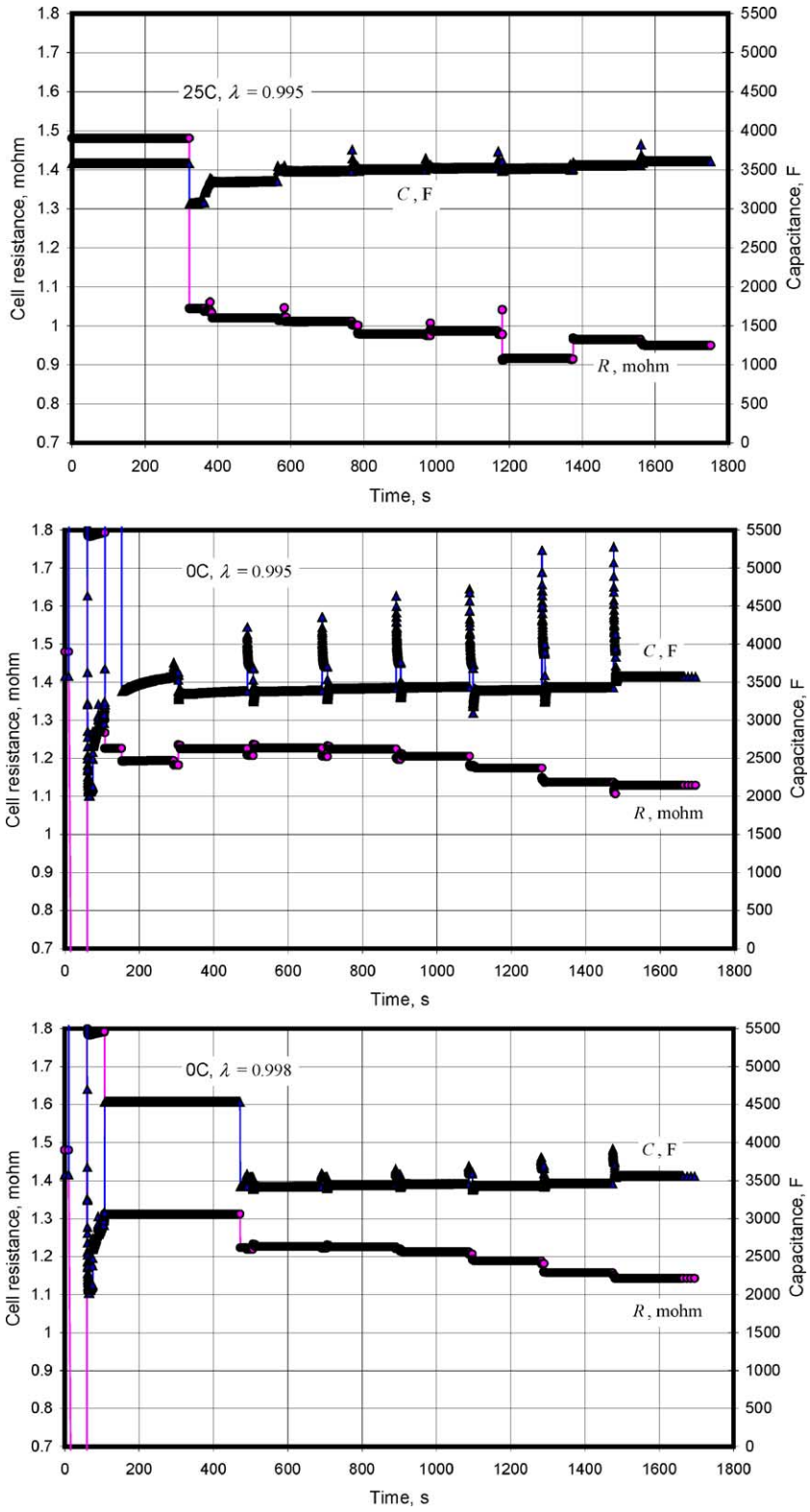

Fig. 13. Extracted (charge) parameters and the effect of the forgetting factor λ.

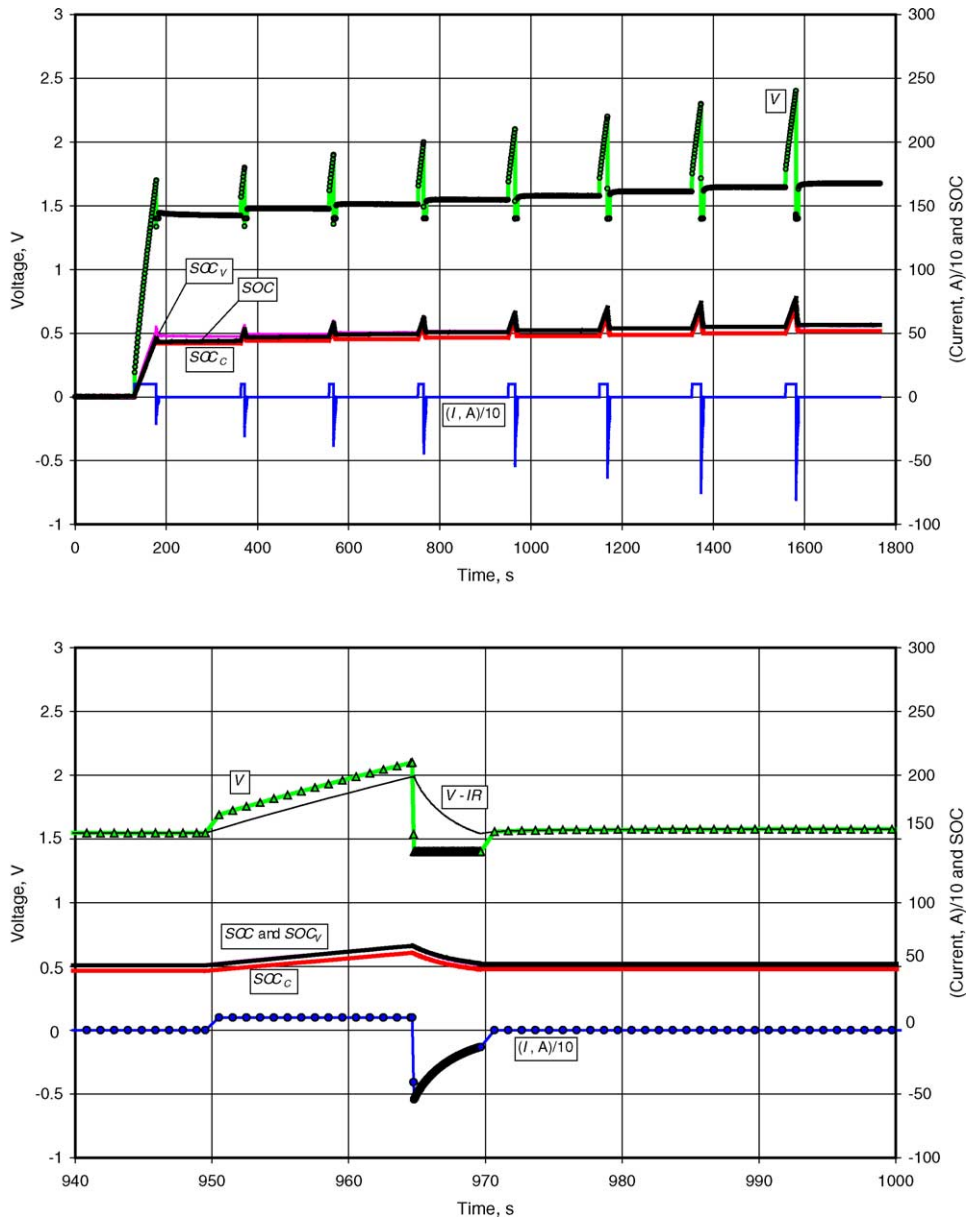

Fig. 14. Discharge power test (cf. Table 1) at 25 °C. The extracted state of charge (SOC) from the adaptive algorithm is indicated, as is the voltage-based contribution (SOC_V) and that corresponding to purely coulomb counting (SOC_C). The lower plot expands the time axis about 970 s and allows one to view the constant current (100 A discharge) prior to the voltage step to 1.4 V, the minimum voltage, which gives rise to the maximum discharge power (*IV*).

simplicity of the RC circuit does not allow one to understand the underlying phenomena that govern the potential–current relationship, the successful correlation of the capacitor behavior does bode well for the use of the RC circuit for the construction of an adaptive filter and ultimately an adaptive algorithm. More complex models that include the numerical solution to coupled partial differential equations for the purposes of describing thermodynamic, kinetic, and transport phenomena from a microscopic basis are required to improve the design and performance of activated-carbon electric-double-layer capacitors. A comparison of the RC circuit as a model versus its use as an adaptive filter is provided in Fig. 9 (with an expanded abscissa shown in Fig. 10). In both plots, the measured current and voltage are shown by the solid lines. The current source was constructed so as to be similar that which would be used in a capacitor-based system in an automotive application. In the upper plot is the curve depicting the model voltage (symbols) constructed by the model equation (cf. Eq. (4)):

$$V|_N = (t_N - t_{N-1})\frac{I|_N + I|_N}{2}\frac{1}{C} + I|_N R + (V|_{N-1}^{\text{calculated}} - |_{N-1} R),$$

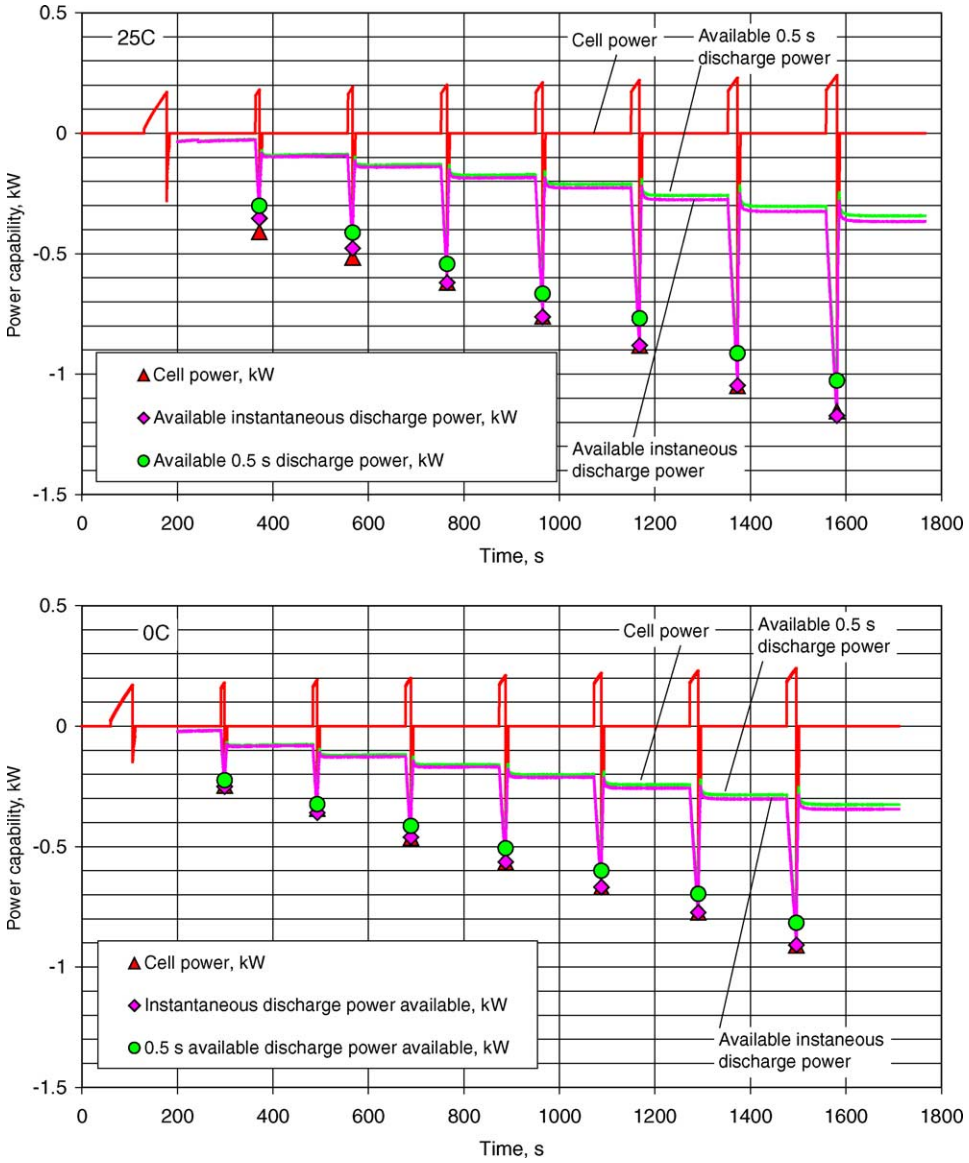

Fig. 15. Available discharge power analysis for 25 °C (upper plot) and 0 °C (lower plot). The algorithm utilizes the current and voltage traces shown in the upper plot of Fig. 14 to produce the available discharge power results depicted above. The available discharge power predictions rendered by the recursive algorithm follow closely the measured power through the voltage reversals (i.e., through the transition from a constant 100 A charge to a 1.4 V step). For these analyses, $\lambda = 0.995$. Lower discharge powers are available as the temperature is decreased, consistent with the results of Fig. 8.

whereas the voltage displayed by the symbols in the lower plot corresponds to the adaptive filter,

$$V|_N = (t_N - t_{N-1})\frac{I|_N + I|_{N-1}}{2}\frac{1}{C} + I|_N R + (V|_{N-1}^{\text{measured}} - I|_{N-1}R).$$

The above two equations differ only in the voltage term V_{N-1}. The comparison of the two plots makes it clear that while the use of Eq. (4) is not appropriate for general application, the implementation of Eq. (4) as an adaptive filter does provide a relatively good representation of the voltage response, and the extracted parameters deduced from the adaptive filter resemble values reported in the previous section. Thus, as is commonly the case in the construction of model-reference adaptive systems, the very basic model provides a crude approximation to the system behavior, while the recasting of the model as an adaptive, transversal filter [28] provides a valuable result.

4.3. Adaptive algorithm results

The explicit outputs from the adaptive algorithm are the (i) state of charge, (ii) the charge and discharge power capability, and (iii) the regressed parameters (R and C, which can be used to deduce the state of health of the system). Results for the

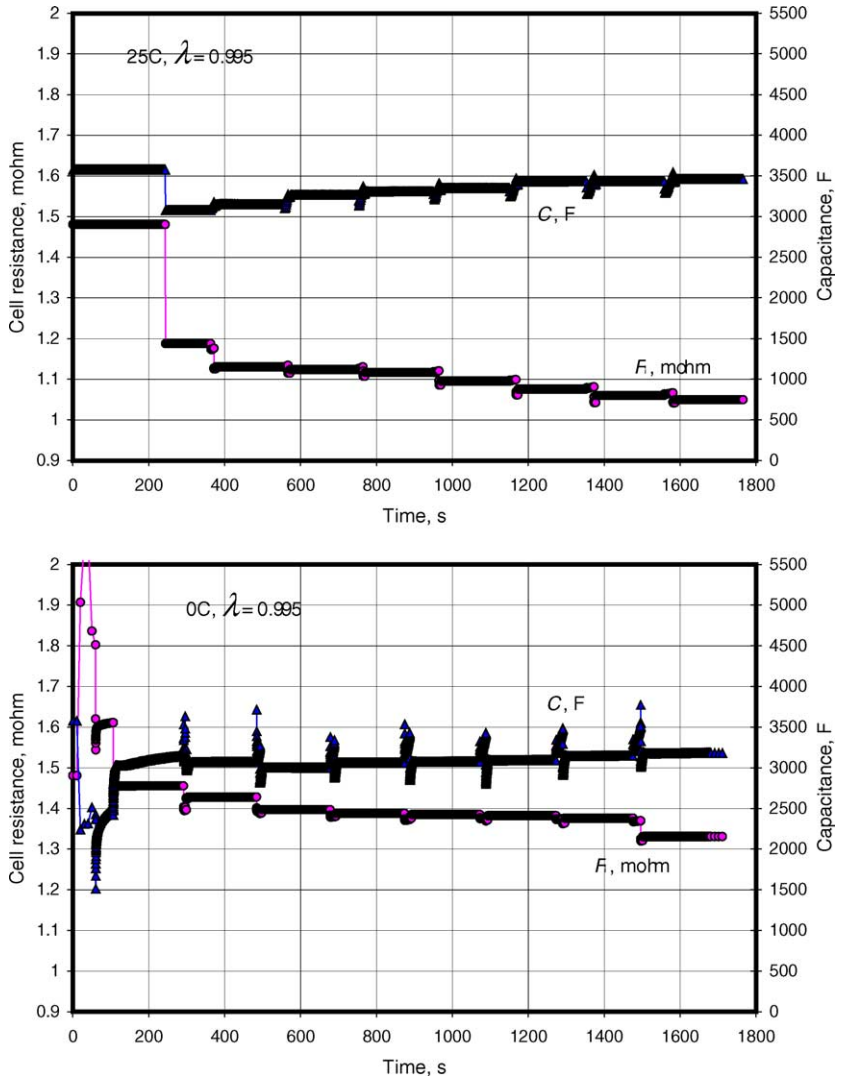

Fig. 16. Extracted (discharge) parameters. The parameter values can be compared with those depicted in Fig. 13 for the charge analysis. The extracted resistance R is larger than that of Fig. 13, consistent with the SOC being lower for the discharge tests (Fig. 14, about 50% SOC at end of test) than for the charge tests (Fig. 11, about 90% SOC at end of test); the same trend for the R vs. SOC relationship is seen in the lower panel of Fig. 6. Although less pronounced, the same explanation applies to the extracted capacitance C (cf., Fig. 4).

tests labeled "Discharge power test" and "Charge power test" in Table 1 are displayed Figs. 11–16.

The performance of the adaptive algorithm with respect to predicting the energy left in the system, identified with the SOC, is depicted in Fig. 11. In the upper plot, we see that the algorithm returns a value close to that obtained using simply coulomb counting ($w = 1$ in Eq. (11)). This use of purely coulomb counting to assess the accuracy of an adaptive algorithm over time scales long relative to convergence of the algorithm but short relative to the influence of current inefficiencies (side reactions [2,17]) has been shown to be a useful evaluation method. For longer durations, as in actual vehicle applications, purely coulomb counting will become substantially inaccurate due to current inefficiencies. The duration for convergence for the chosen set of parameters is indicated by the lower plot in Fig. 11, where the starting SOC for the algorithm was set arbitrarily to 25%, instead of the correct value of zero, consistent with the starting state of equilibration at 0 V. After about 1400 s the voltage-based SOC is nearly identical to that of the combined SOC. For this analysis, unless otherwise noted, $w = 0.999$, indicating a very stable algorithm greatly influenced by SOC_I. The algorithm can be made more adaptive (and less stable) by lowering w.

The prediction of the capacitor's power capability associated with subjecting the discharging (at 100 A) capacitor to an abrupt maximum charge condition (2.8 V) is demonstrated in Fig. 12. Generally excellent results are obtained, indicating that the algorithm and the power capability Eqs. (12)–(14) work quite well. The lower plot in Fig. 12 displays an expanded abscissa; the fact that the solid line, reflecting the actual power, tends to the curve represented by the symbols (predicted charge power capability) when the

potential is abruptly set to 2.8 V, corresponding to a current and power reversal, implies that the algorithm correctly captures the maximum charge power available for this rather severe test case. The charge power prediction is always greater than that extrapolated by Eq. (14) when $\Delta t = 500$ ms and is close to the instantaneous charge power extrapolation, Eq. (13).

The regressed parameters R and C are shown in Fig. 13. The variation in the extracted parameters can be reduced by decreasing the forgetting factor, as is shown in the lower plot of Fig. 13 for the 0 °C condition; however, longer convergence times are then expected. The general lack of temperature sensitivity can be seen by comparing the 0 and 25 °C results in Fig. 13; because the results tended to be quite similar over the temperature range of −30 to 45 °C, in terms of algorithm performance, most of the algorithm analysis is provided for the 25 °C condition only.

The analogous experiments to investigate the discharge-power prediction capability are shown in Figs. 14, 15 and 16. Again, 0 and 25 °C data are analyzed, and similar values for R and C are obtained. As with the test of the charge-power prediction capability, the discharge power prediction is always greater than that extrapolated by Eq. (14) when $\Delta t = 500$ ms and is close to the instantaneous discharge power extrapolation, Eq. (12).

5. Summary and conclusions

1. *A series of tests (cf. Table 1) were completed to characterize electrochemically the performance of a promising electric-double-layer capacitor*: the characterization relies on a simplified equivalent circuit interpretation extracted from a more-complete mathematical representation of the capacitor system. The simplified model amounts to a series RC circuit, and the resistance R and capacitance C are extracted over the temperature range of interest for automotive applications (−30 to 45 °C). A variety of tests yielded consistent values for R and C, indicating that the simple model is sufficient for our purposes. The robustness of the equivalent circuit enables the formulation of an associated model-reference adaptive algorithm: the measured values of R and C allow one to place reasonable bounds on the adapted values of these parameters and assess whether the capacitor system is functioning appropriately in a vehicle application (i.e., deduce the state of health of the capacitor system).
2. *In addition to the high power capability and potentially low costs of this class of capacitors, we clarify the substantial invariance of the device performance with respect to temperature, a distinct advantage over battery systems*: however, these three attributes, relative to batteries, come at the sacrifice of energy, a deficiency that renders capacitors better suited to supplement fuel cell systems rather than internal combustion engines, as a fuel cell can be the source of efficient energy.
3. *A computationally efficient adaptive algorithm based on weighted recursive least squares is described and tested*: the algorithm is fully recursive in that the only variables required for on-line regression are those of the previous time step and the current time step. A time-weighting technique, often referred to as exponential forgetting, is employed to damp exponentially the influence of older data points on the regression analysis. Successful comparisons of the algorithm's adapted state of charge and power predictions provide an initial validation of the algorithm.

References

[1] M.W. Verbrugge, E.D. Tate, J. Power Sources 126 (2004) 236.
[2] B.E. Conway, Electrochemical Supercapacitors: Scientific Fundamentals and Technological Applications, Kluwer Academic/Plenum, New York, NY, 1999.
[3] S. Buller, E. Karden, D. Kok, R.W. DeDoncker, IEEE Trans. Ind. Appl. 38 (2002) 1622.
[4] A. Chu, P. Braatz, J. Power Sources 112 (2002) 236.
[5] D.Y. Jung, Y.H. Kim, S.W. Kim, S.-H. Lee, J. Power Sources 114 (2003) 366.
[6] S. Pillar, M. Perrin, A. Jossen, J. Power Sources 96 (2001) 113.
[7] M. Verbrugge, D. Frisch, B. Koch, A generalized approach for adaptive energy management of electric and hybrid electric vehicles, in: Proceedings Volume for the 4th International Advanced Automotive Battery Conference, San Francisco, June 1–4, 2004.
[8] M.W. Verbrugge, P. Liu, S. Soukiazian, Electrochemical characterization and control of supercapacitors, in: Proceedings Volume for the World Summit on Advanced Capacitors, Washington, DC, August, 2004.
[9] M. Ue, K. Ida, S. Mori, J. Electrochem. Soc. 141 (1994) 2989.
[10] M. Ue, M. Takeda, A. Toriumi, A. Kominato, R. Hagiwara, Y. Ito, J. Electrochem. Soc. 150 (2003) A499.
[11] G. Sandi, N.R. Khalili, W. Lu, J. Prakash, J. Power Sources 119–121 (2003) 34.
[12] X.W. Huang, Z.W. Xie, X.Q. He, H.Z. Sun, C.Y. Tong, D.M. Xie, Synth. Met. 135–136 (2003) 235.
[13] C. Kim, J.-S. Kim, S.-J. Kim, W.-J. Lee, K.-S. Yang, J. Electrochem. Soc. 151 (2004) A769.
[14] M.W. Verbrugge, Supercapacitors and automotive applications, in: Proceedings Volume for the World Summit on Advanced Capacitors, Washington, DC, 2003.
[15] M. Endo, Y.J. Kim, H. Ohta, K. Ishii, T. Inoue, T. Hayashi, Y. Nishimura, T. Maeda, M.S. Dresselhaus, Carbon 40 (2002) 2613.
[16] B. Pillay, Design of electrochemical capacitors for energy storage, Ph.D. Dissertation, University of California, Berkeley, 1996.
[17] B. Pillay, J. Newman, J. Electrochem. Soc. 143 (1996) 1806.
[18] K.E. Thomas, R.M. Darling, J. Newman, Mathematical modeling of lithium batteries, in: W. van Schalkwaijk, B. Scrosati (Eds.), Advances in Lithium-Ion Batteries, Kluwer Academic/Plenum, 2002 (Chapter 12).
[19] V. Srinivasan, J.W. Weidner, J. Electrochem. Soc. 146 (1999) 1650.
[20] D. Dunn, J. Newman, J. Electrochem. Soc. 147 (2000) 820.
[21] C. Lin, J.A. Ritter, B.N. Popov, R.E. White, J. Electrochem. Soc. 146 (1999) 3168.
[22] C. Lin, B.N. Popov, H.J. Ploehn, J. Electrochem. Soc. 149 (2002) A167.
[23] H. Kim, B.N. Popov, J. Electrochem. Soc. 150 (2003) A1153.
[24] S. Devan, V.R. Subramanian, R.E. White, J. Electrochem. Soc. 151 (2004) A905.

[25] I.J. Ong, J. Newman, J. Electrochem. Soc. 146 (1999) 4360.
[26] P.S. Maybeck, Stochastic Models. Estimation and Control of Mathematics in Science and Engineering, vol. 141–151, Academic Press, 1979.
[27] A. Gelb (Ed.), Applied Optimal Estimation, MIT Press, Cambridge, MA, 1974.
[28] B. Widrow, S.D. Stearn, Adaptive Signal Processing, Prentice-Hall, Englewood Cliffs, NJ, 1985.
[29] L. Ljnug, T. Söderström, Theory and Practice of Recursive Identification, MIT Press, 1986.
[30] K.J. Åström, B. Wittenmark, Adaptive Control, Addison-Wesley, 1989.
[31] B.D.O. Anderson, J.B. Moore, Optimal Filtering, Prentice-Hall, Englewood Cliffs, NJ, 1979.
[32] R. Kulhavý, Recursive Nonlinear Estimation. A Geometric Approach, Springer, London, 1996.